Chinese Journal of Natural Medicines

Discovery of bioactive constituents from *Inula britannica* and their anti-pneumonia effects

Na Wang, Siwen Hui, Jianbo Sun, Xinrong Xu, Huilin Zhang, Jing Chang, Qimeng Zhu, Yaxue Jia, Xiaohong Shu, Juan Zhang, Chengpeng Sun

Citation: Na Wang, Siwen Hui, Jianbo Sun, Xinrong Xu, Huilin Zhang, Jing Chang, Qimeng Zhu, Yaxue Jia, Xiaohong Shu, Juan Zhang, Chengpeng Sun, Discovery of bioactive constituents from *Inula britannica* and their anti-pneumonia effects, Chinese Journal of Natural Medicines, 2026, 24(7), 887-896. doi: 10.1016/S1875-5364(26)61192-2.

View online: https://doi.org/10.1016/S1875-5364(26)61192-2

Related articles that may interest you

Polysaccharides from Chinese herbal medicine: a review on the hepatoprotective and molecular mechanism
Chinese Journal of Natural Medicines. 2024, 22(1), 4-14 https://doi.org/10.1016/S1875-5364(24)60558-3

The bioinformatics and metabolomics research on anti-hypoxic molecular mechanisms of Salidroside *via* regulating the PTEN mediated PI3K/Akt/NF-κB signaling pathway
Chinese Journal of Natural Medicines. 2021, 19(6), 442-453 https://doi.org/10.1016/S1875-5364(21)60043-2

Chemical profiling of Huashi Baidu prescription, an effective anti-COVID-19 TCM formula, by UPLC-Q-TOF/MS
Chinese Journal of Natural Medicines. 2021, 19(6), 473-480 https://doi.org/10.1016/S1875-5364(21)60046-8

Isolation and microbial transformation of tea sapogenin from seed pomace of *Camellia oleifera* with anti-inflammatory effects
Chinese Journal of Natural Medicines. 2024, 22(3), 280-288 https://doi.org/10.1016/S1875-5364(24)60598-4

Anti-psoriasis molecular targets and active components discovery of Optimized Yinxieling Formula *via* affinity-purified strategy
Chinese Journal of Natural Medicines. 2024, 22(2), 127-136 https://doi.org/10.1016/S1875-5364(24)60563-7

Honokiol: A naturally occurring lignan with pleiotropic bioactivities
Chinese Journal of Natural Medicines. 2021, 19(7), 481-490 https://doi.org/10.1016/S1875-5364(21)60047-X

Wechat

Chinese Journal of Natural Medicines 24 (2026) 887-896

Contents lists available at ScienceDirect

Chinese Journal of Natural Medicines

journal homepage: www.cjnmcpu.com/

Original article

Discovery of bioactive constituents from *Inula britannica* and their anti-pneumonia effects

Na Wang[a,Δ], Siwen Hui[a,Δ], Jianbo Sun[a,b], Xinrong Xu[a], Huilin Zhang[a,b], Jing Chang[a], Qimeng Zhu[a], Yaxue Jia[a], Xiaohong Shu[b,*], Juan Zhang[a,*], Chengpeng Sun[a,*]

[a] *School of Chinese Materia Medica, School of Medical Technology, Tianjin Key Laboratory of Therapeutic Substance of Traditional Chinese Medicine, Tianjin University of Traditional Chinese Medicine, Tianjin 301617, China*

[b] *College of Pharmacy, Dalian Medical University, Dalian 116044, China*

ARTICLE INFO

Article history:
Received 4 November 2025
Revised 29 December 2025
Accepted 9 February 2026
Available online 20 July 2026

Keywords:
Inula britannica
Bioactive constituent
Anti-pneumonia effect
Molecular mechanism

ABSTRACT

Pneumonia is a highly prevalent acute respiratory infection worldwide, and *Inula britannica* displayed an anti-pneumonia effect. Herein, twenty compounds were isolated from *I. britannica*, including seven newly discovered compounds—six terpenoids named inulabritanoids P–U (**1**–**6**) and one novel lignan, inulabritanoid V (**7**)—along with thirteen known compounds (**8**–**20**). Their structural frameworks were clarified through 1D and 2D NMR, and HR-MS data. Effects of all the elucidated compounds for anti-pneumonia activities were assessed using the lipopolysaccharide (LPS)-induced pneumonia model in MH-S alveolar macrophages. Compounds **3**, **5**, **6**, **12**, and **18** showed potent anti-pneumonia activities in LPS-exposed MH-S cells. Notably, compound **6** exhibited the most potent bioactivity: it significantly inhibited nitric oxide (NO) production and downregulated the expression levels of inflammatory factors tumor necrosis factor-α (TNF-α), interleukin-1α (IL-1α), IL-6, and chemokine (C-C motif) ligand 5 (CCL5). Further investigations revealed that the anti-pneumonia effect of compound **6** depended on inhibiting the NF-κB and MAPK/AP-1 signaling pathways. These results indicate that compound **6** represents a viable lead molecule for combating pneumonia, laying a foundation for future studies.

1. Introduction

Pneumonia is a globally prevalent acute respiratory infection with high incidence [1, 2]. There is an urgent clinical need for anti-pneumonia candidates with clear anti-inflammatory activity and good safety [3]. Its pathological progression is closely linked to aberrant activation of NF-κB and MAPK pathways [4-8], which act as core hubs regulating inflammatory dysregulation in pneumonia [9]. Upon NF-κB activation, its core protein p65 is phosphorylated and translocates into the nucleus, where it directly regulates the transcription of inflammatory cytokines such as TNF-α and IL-1α, resulting in abundant release of inflammatory mediators [10-13]. Simultaneously, the MAPK/AP-1 pathway, primarily including p38, ERK, and JNK, is activated; it amplifies inflammatory signals by phosphorylating downstream activator protein-1 (AP-1, a complex of c-Jun/c-Fos) [14-16], thereby exacerbating inflammatory cell infiltration in lung tissue [17]. Synergistic overactivation of these two pathways triggers an inflammatory cascade, ultimately driving pneumonia progression toward severe outcomes such as respiratory failure. This confirms NF-κB and MAPK pathways as core therapeutic targets for anti-inflammatory intervention in pneumonia [18-22].

Traditional Chinese medicine (TCM) represents a unique therapeutic strategy for treating and preventing pneumonia, with a long history of clinical application. Ouya Xuanfu Hua is the Chinese name for the medicinal plant *Inula britannica*. Its flowers are listed in *Chinese Pharmacopoeia* as well as having been proven to exhibit significant anti-inflammatory, antioxidant, lung-protective, and antimicrobial characteristics [23-28]. Furthermore, *I. britannica*, which is recorded in classic TCM formula (Xuanfu Daizhe Tang), is commonly used for treating upper respiratory tract infections, pneumonia, and other febrile diseases [25, 29].

To systematically clarify the pharmacodynamic material basis and mechanism of action of *I. britannica* for treating pneumonia, this study successfully isolated and identified seven new compounds inulabritanoids P–V (**1**–**7**, Fig. 1) and thirteen known compounds (**8**–**20**). Their structures were unequivocally characterized through comprehensive spectroscopic analysis [30]. Meanwhile, their anti-pneumonia effects were assayed using lipopolysaccharide (LPS)-mediated pneumonia MH-S cell model, and their potential mechanisms were studied. This study aimed to establish a scientific foundation and identify candidate compounds for developing new anti-pneumonia drugs derived from natural products.

2. Results and discussion

2.1. Structural elucidation

Inulabritanoid P (**1**) was assigned the molecular formula of

* Corresponding author.
E-mail addresses: xiaohong_shu@dmu.edu.cn (X. Shu); zhangj_428@163.com (J. Zhang); suncp146@163.com (C. Sun)
Δ These authors contributed equally to this work.

https://doi.org/10.1016/S1875-5364(26)61192-2
Copyright © 2026, China Pharmaceutical University. Published by Elsevier B.V. All rights are reserved.

$C_{20}H_{30}O_4$ revealed by ^{13}C NMR and positive HR-MS (observed *m/z* 335.2211 $[M + H]^+$, Calcd. for $C_{20}H_{31}O_4^+$, 335.2222) data. Its ^1H NMR spectrum (600 MHz, CD_3OD, Table 1) exhibited two olefinic hydrogen signals [δ_H 5.27 (1H, br s) and 5.17 (1H, br s)] and two oxygen-connected protons [δ_H 3.78 (1H, m) and 3.67 (1H, s)] as well as two methyl signals [δ_H 1.21 (3H, s) and 0.95 (3H, s)]. Analysis of its ^{13}C NMR (150 MHz, CD_3OD, Table 1) data revealed twenty distinct carbon resonances. Key signals were assignable to a carboxyl signal (δ_C 181.7), two olefinic signals (δ_C 155.2 and 112.2), two oxygenated signals (δ_C 83.7 and 72.1), and two methyl signals (δ_C 29.6 and 16.9). The NMR spectral characteristics of **1** are highly consistent with those previously reported for noueinsiancin D isolated from *Nouelia insignis* [31], whereas their differences at C-15, C-16, and C-17 were attributed to a hydroxy group (δ_C 72.1) in **1** substituting for the carbonyl group (δ_C 226.2) in noueinsiancin D, and an exocyclic olefinic functionality (δ_C 155.2 and 112.2) in **1** instead of the ethyl group (δ_C 42.9 and 11.7) in noueinsiancin D. Subsequent HMBC-related signals (H_2-17 to C-15/C-16; H-15 to C-17; Fig. 2) supported this structural assignment. The NOESY data finally established the relative stereo-configuration of **1** through significant cross-spatial interactions (Fig. 3). Key correlations from H-9 with H-12/H-15, H_3-20 with H-11a/H-1a, H-9/H-5 with H-1b/H_3-19, and H_2-14 with H-13/H-11a indicated that R^* configurations of C-8 and C-13, an S^* configuration of C-9 were ultimately designated, H_3-20/OH-12/OH-15 were α-oriented, and H_3-19/H-5/H-9 were β-oriented.

HR-MS and ^{13}C NMR data have undoubtedly confirmed that the molecular formula of inulabritanoid Q (**2**) was actually $C_{20}H_{32}O_4$. HR-MS displayed a peak at *m/z* 335.2221 $[M - H]^-$ (calcd. for $C_{20}H_{31}O_4^-$, 335.2222). The ^1H and ^{13}C NMR spectra of **2** (600/150 MHz, CD_3OD) revealed a profile closely related to those of **1** (Table 1). Their discrepancy resided in the structural fea-

Table 1 ^1H (600 MHz) and ^{13}C NMR (150 MHz) data of compounds **1**–**3**.

No.	**1**[a]		**2**[a]		**3**[b]	
	δ_C	δ_H (*J* in Hz)	δ_C	δ_H (*J* in Hz)	δ_C	δ_H (*J* in Hz)
1	42.1	1.90, m	50.9	2.20, m	41.6	2.54, dd, (18.7, 6.0)
		0.86, m		0.70, m		2.08, br d, (18.7)
2	20.5	1.89, m	65.2	4.09, m	147.3	6.85, ddd, (9.6, 6.8, 2.5)
		1.42, m				
3	39.3	2.15, m	47.8	2.40, m	127.9	5.90, dd, (10.0, 2.8)
		1.03, td, (14.3, 4.1)		0.93, m		
4	44.9		45.9		200.2	
5	58.2	1.10, m	57.8	1.03, m	55.5	2.23, dd, (11.8, 2.8)
6	22.3	1.93, m	23.5	1.79, m	17.6	1.82, m
		1.77, m				1.19, m
7	36.0	1.76, m	42.9	1.45, m	32.1	1.60, dt, (13.8, 6.1, 2.8)
		1.38, m				1.31, m
8	48.6		46.0		46.6	
9	55.4	1.10, m	56.8	1.05, m	50.3	1.40, m
10	40.6		42.2		41.8	
11	29.0	1.78, m	20.2	1.68, m	17.8	1.46, m
		1.11, m				1.43, m
12	72.1	3.78, m	32.6	1.56, m	31.9	1.54, m
				1.45, m		1.41, m
13	50.9	2.63, m	39.7	2.08, m	41.6	2.65, m
14	36.1	1.89, m	38.2	1.83, m	35.3	1.71, br d, (11.4)
		1.48, dd, (12.1, 5.7)		1.02, m		1.33, m
15	83.7	3.67, s	46.4	1.55, m	80.9	3.66, s
				0.91, m		
16	155.2		44.5	1.93, m	159.3	
17	112.2	5.27, br s	67.8	3.77, m	107.8	5.10, br s
		5.17, br s		3.30, m		4.99, br s
18	181.7		181.2		15.5	0.91, s
19	29.6	1.21, s	29.6	1.24, s		
20	16.9	0.95, s	17.0	0.97, s		

[a] Measured in CD_3OD; [b] Measured in DMSO-d_6.

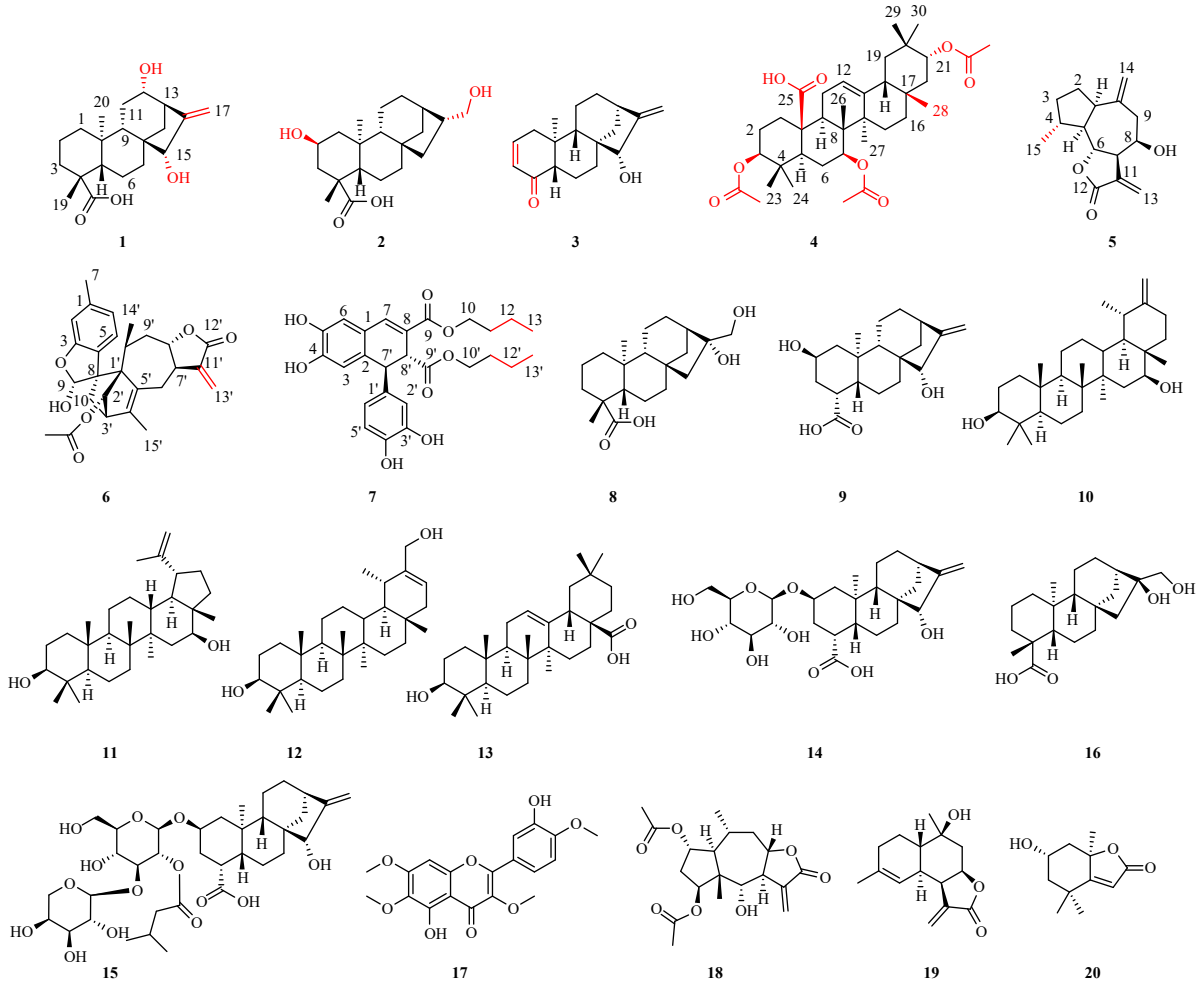


Fig. 1 Chemical structures of compounds **1**–**20**.

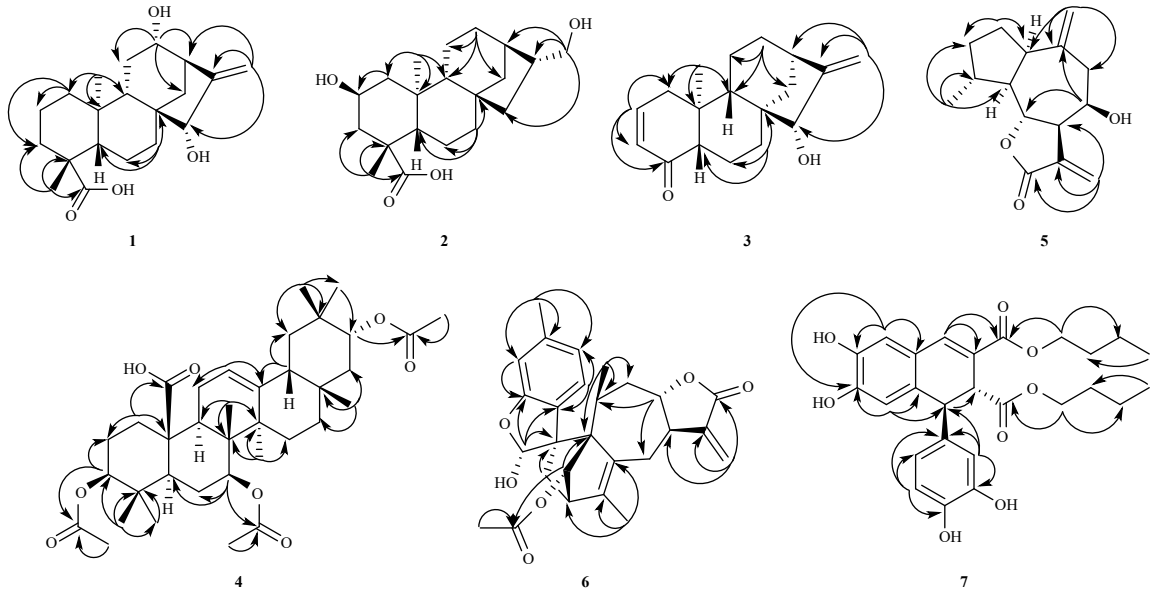


Fig. 2 Key HMBC correlations of compounds **1**–**7**.

tures at positions C-16, C-15, C-12, C-2, and C-17. A hydroxymethyl group (δ_C 67.8) was identified in **2**, while **1** featured two hydroxyl groups (δ_C 72.1 and 83.7) and an exocyclic olefinic bond (δ_C 155.2 and 112.2). This presumption was subsequently corroborated by HMBC evidence of H_2-17 to C-13/C-16, H-9 to C-12, and H-1 to C-2 (Fig. 2). Establishment of the configuration for **2** relied on NOESY correlations (H_3-20/H-1a/H-2; H-5/H_3-19; H-9/H-5; H-17b/H-15b/H-13; H-9/H-15a, Fig. 3), suggesting a co-facial orientation of the involved protons. Consequently, (8S^*,13R^*)-configuration, an α-orientation of H_3-20 and β-orientations of H-5, OH-

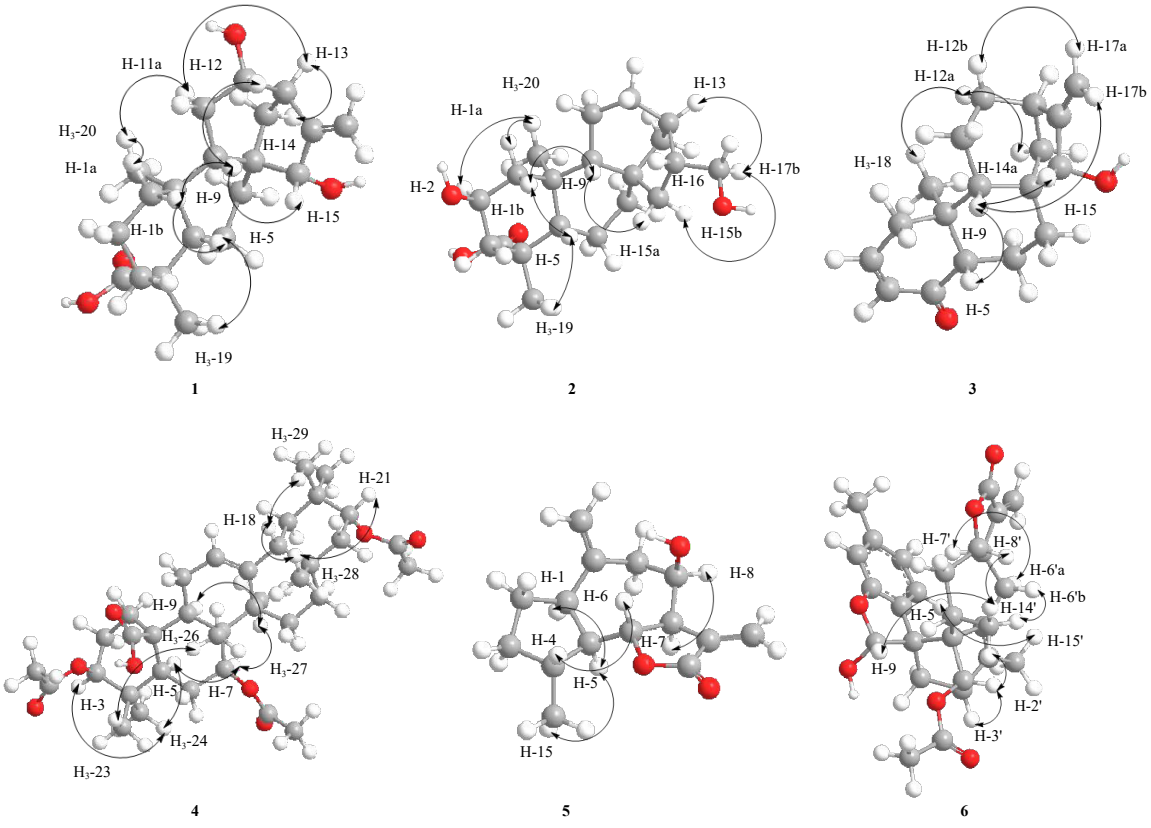


Fig. 3 Key NOESY correlations of compounds **1**–**6**.

2, H-16, H-9, and H$_3$-19 were assigned.

Positive HR-MS and ^{13}C NMR data established beyond doubt the molecular formula as $C_{18}H_{24}O_2$ for inulabritanoid R (**3**). Analysis of ^{1}H and ^{13}C NMR data for **3** and **1** demonstrated a striking structural similarity. Their structural variances were identified as follows: the hydroxy group at C-12 in **1** was absent in **3**, and the corresponding carbon resonance was shielded (δ_C 72.1 in **1** to 31.9 in **3**), the methyl carbon at C-4 (δ_C 29.6) and carboxyl carbon (δ_C 181.7) at C-25 in **1** were replaced by a carbonyl in **3** and a double bond between C-2 and C-3 was established in **3**, along with a significant deshielding of the C-4 signal. The carbon resonances for C-2/C-3 shifted downfield from δ_C 39.3 and 20.5 in **1** to δ_C 147.3 and 127.9 in **3**, while the C-4 resonance moved from δ_C 44.9 in **1** to δ_C 200.2 in **3**. The above deductions were revealed by HMBC cross-peaks from H-9 to C-12, and H-3 to C-4/C-2 (Fig. 2). In addition, its configuration was determined *via* the NOESY spectroscopy showing correlations of H-9/H-15/H-5, H$_3$-18/H-12a, H-12a/H2-14, and H-17a/H-12b/H-9 (Fig. 3), suggesting that H$_3$-18 and OH-15 were established to exhibit an α-orientation, H-5 and H-9 were established to adopt a β-orientation, and (8R^*,13R^*)-configuration was thus unambiguously assigned. In order to determin the absolute configuration of **3**, quantum chemical calculations were performed. As shown in Fig. 4, the calculated ECD spectrum of 5*S*,8*R*,9*S*,10*S*,13*R*,15*S*-**3** agreed with its experimental ECD spectrum (Fig. 4), which indicated its absolute configuration.

Based on positive HR-MS data at *m/z* 613.3746 [M – H]$^-$ (Calcd. for $C_{36}H_{53}O_8^-$, 613.3740), the molecular composition of inulabritanoid S (**4**) was $C_{36}H_{54}O_8$. The NMR data of **4** revealed that it shared an oleanane-type triterpenoid skeleton. Comparison of its NMR data with those of oleanolic acid indicated that **4** had more three acetyl groups (δ_C 171.1, 171.0, 170.6, 28.5, 22.1, and 21.4) than oleanolic acid, and the carboxyl group in **4** was located at C-25 (δ_C 179.7) rather than at C-28 (δ_C 181.0) in oleanolic acid [32]. This conduction was supported by correlations of H-21 to OAc-21, H-3 to OAc-3, H-7 to OAc-7, H-9 to C-25, and H$_3$-28 to C-17/C-16/C-22 in its HMBC spectrum (Fig. 2). Key NOESY interactions of H$_3$-24 with H-5/H-3, H-9 with H-7/H$_3$-27/H-5, and H$_3$-29 with H-18/H$_3$-28/H-21 (Fig. 3) implied β-orientations of OAc-3, OAc-7, H$_3$-23, H$_3$-26, H$_3$-29, H$_3$-28, and H-18 and α-orientations of OAc-21, H-5, H-9, H$_3$-24, and H$_3$-27.

Inulabritanoid T (**5**) had a molecular formula of $C_{15}H_{20}O_3$, as evidenced by means of its ^{13}C NMR and HRMS data. Its NMR data suggested the similarity with (1*R*,4*R*,5*S*,6*R*,7*R*,8*S*)-8,15-dihydroxyguaia-10(14),11(13)-dien-12,6-olide [33]. The critical differences lied in the substitution of a methyl group (δ_C 20.2) in **5** for the hydroxymethyl group (δ_C 66.1) in (1*R*,4*R*,5*S*,6*R*,7*R*,8*S*)-8,15-dihydroxyguaia-10(14),11(13)-dien-12,6-olide, the C-4 res-

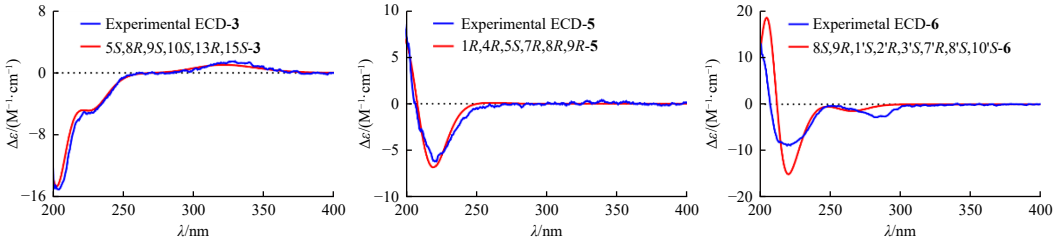


Fig. 4 Experimental and calculated ECD spectra of compounds **3**, **5**, and **6**.

onance was observed at a significantly downfield shift (δ_C 49.4) compared to its position in **5** (δ_C 38.8), which was supported by HMBC cross-peaks (H_3-15 to C-3/C-4/C-5; Fig. 2). Key spatial correlations of H-5 with H-1/H-7/H_3-15, and H-6/H-4, and H-7/H-8 were observed in the NOESY spectrum (Fig. 3), supporting *α*-orientations for H-1, H-5, H-7, and H_3-15, and *β*-orientations for H-6, H-4, and OH-8. (1*R*,4*R*,5*S*,7*R*,8*R*,9*R*)-configuration was determined based on the quantum chemical calculation (Fig. 4).

Inulabritanoid U (**6**) possessed a molecular formula as $C_{27}H_{30}O_6$ depended on its ^{13}C NMR and HR-MS data. The NMR characteristics data of **6** were highly comparable to those of dibritannilactone A [34]. Their main distinction was the presence of the $\Delta^{11'(13')}$ exocyclic olefinic bond in **6**. This structural difference was validated by the upfield shifts observed at C-11' (δ_C 39.9) and C-13' (δ_C 9.7) in dibritannilactone A, compared to their positions in **6** (δ_C 139.9 and 118.0). In its HMBC spectrum, correlations of H-13a' to C-11'/C-12'/C-7' were used to determine the location of the $\Delta^{11'(13')}$ exocyclic olefinic bond (Fig. 2). Further NOESY analysis determined its relative stereochemistry through key correlations: H_3-14'/H-9; H-2'/H-3'/H_3-14'/H-8'; H-5/H_3-15'; H-7'/H-6'a; and H_3-14'/H-6'b (Fig. 3), suggesting *β*-orientations of H_3-14', H-8', and H-9 and *α*-orientations of OH-9, OAc-2', and H-7'. The absolute configuration of **6** was defined as 8*S*,9*R*,1'*S*,2'*R*,3'*S*,7'*R*,8'*S*,10'*S* through a comparison of experimental and calculated ECD spectra of **6** (Fig. 4).

HR-ESI-MS analysis of inulabritanoid V (**7**) generated an $[M + H]^+$ ion at *m/z* 471.2020 (Calcd. for $C_{26}H_{31}O_8^+$, 471.2019), suggesting its molecular formula as $C_{26}H_{30}O_8$. Interpretation of the HSQC and HMBC NMR spectra revealed that **7** was an aryl dihydronaphthalene. Evaluation of the NMR data between **7** and the known (7'*S*,8'*R*)-4,5,3',4'-tetrahydroxy-2,7'-cyclolign-7-ene-9,9'-dioic acid diethyl ester revealed key differences at side chain of C-9 and C-9' [35]. Characteristic ^{13}C NMR data was observed at δ_C 64.0, 63.8, 30.3, 30.1, 18.6, 18.4, 13.6, and 13.6, which demonstrated the presence of two *n*-butyl groups in **7**. Their locations were determined based on HMBC cross-peaks of H_2-10 with C-9 and H_2-10' with C-9' (Fig. 2). **7** had the same configuration as (7'*S*,8'*R*)-4,5,3',4'-tetrahydroxy-2,7'-cyclolign-7-ene-9,9'-dioic acid diethyl ester according to its NOESY spectrum.

Additionally, thirteen known compounds (**8**–**20**) were obtained from *I. britannica*, and named as *ent*-16*α*,17-dihydroxy-kauran-19-oic acid (**8**) [36], atractyligenin (**9**) [37], arnidiol (**10**) [38], 3*β*,16*β*-dihydroxylup-20(29)-ene (**11**) [39], taraxast-20-ene-3*β*,30-diol (**12**) [40], oleanolic acid (**13**) [41], 2-*O*-*β*-D-glucopyranosyl actracyligenin (**14**) [42], hupehenoside A (**15**) [36], 17-hydroxy-16*β*-*ent*-kauran-19-oic acid (**16**) [43], casticin (**17**) [44], inuchinenolide C (**18**) [45], cadinanolide (**19**) [46], and loliolide (**20**) [47], respectively.

2.2. Anti-pneumonia assessment

I. britannica is widely employed in China to treat inflammation-mediated pulmonary diseases, such as pneumonia and pulmonary fibrosis, therefore we constructed an LPS-exposed MH-S pneumonia cell model for assaying anti-pneumonia effects of compounds **1**–**20**, and indometacin (Ind) was used as the positive control drug. As shown in Fig. 5A, compounds **3**, **5**, **6**, **12**, and **18** inhibited nitric oxide (NO) production by more than 40% at 10 μmol·L^{-1}, and at 40 μmol·L^{-1} , all except compound 3 maintained an inhibition rate of over 70%. It was worth noting that compound **6** displayed most potent anti-inflammatory effect (83.6%, Fig. 5B). These results indicate anti-pneumonia potentials of compounds **3**, **5**, **6**, **12**, and **18**.

2.3. Compound **6** exhibited anti-pneumonia effect *in vitro*

Next, compound **6** was therefore selected for further investigation. Subsequent ELISA experiments revealed that compound

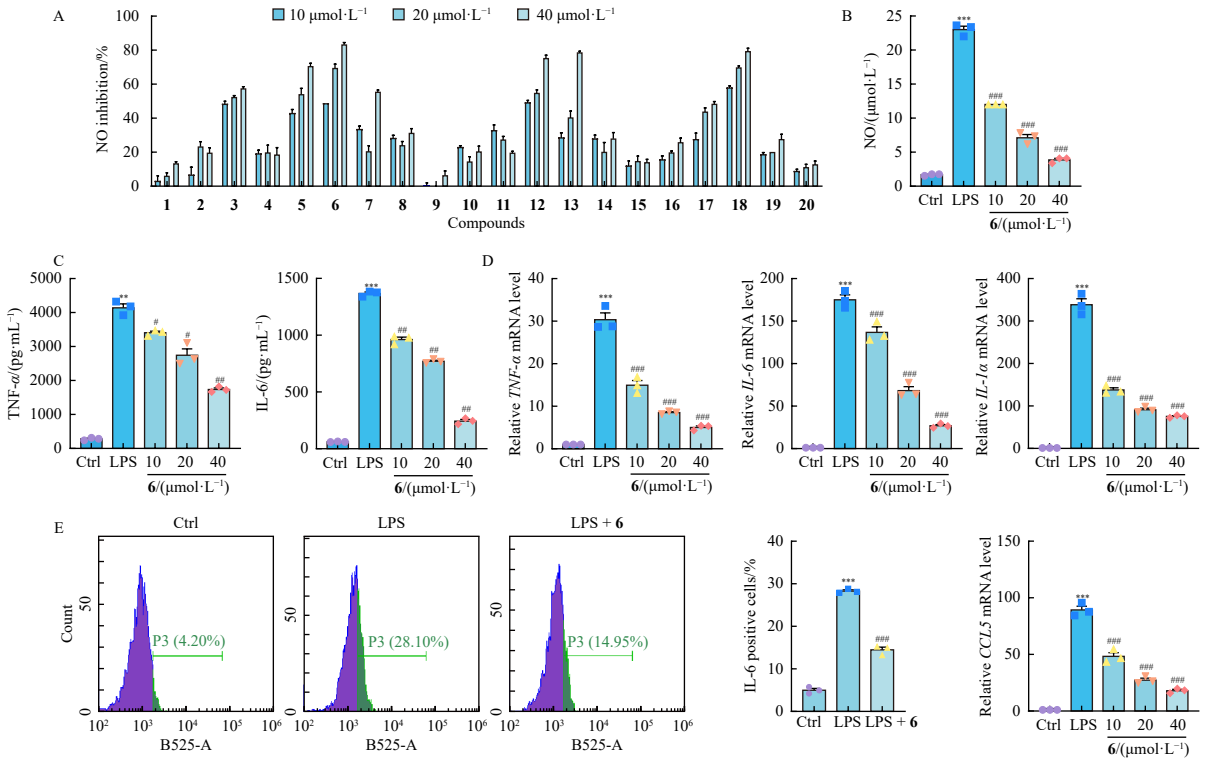


Fig. 5 Compound **6** exhibited anti-pneumonia effect *in vitro*. (A) Anti-pneumonia effects of compounds **1**–**20** at concentrations of 10, 20, and 40 μmol·L^{-1} in LPS-stimulated MH-S pneumonia cell model; (B) Inhibitory effects of compound **6** toward NO production; (C) Levels of TNF-α and IL-6 in the culture supernatants of LPS-stimulated MH-S cells treated with compound **6**; (D) mRNA levels of *TNF-α*, *IL-6*, *IL-1α*, and *CCL5* treated with compound **6**; (E) Flow cytometry analysis of IL-6 expression in LPS-stimulated MH-S cells treated with compound **6**. Data were expressed as mean ± SEM (n = 3). $^{**}P < 0.01$, $^{***}P < 0.001$ *vs* the control group; $^{\#}P < 0.05$, $^{\#\#}P < 0.01$, $^{\#\#\#}P < 0.001$ *vs* LPS group, one-way ANOVA.

6 inhibited the release of inflammatory factors NO, TNF-α, and IL-6 (Fig. 5C). Consistent with these findings, compound **6** markedly decreased mRNA expressions of *IL-1α*, *IL-6*, *TNF-α*, and *CCL5* in LPS-exposed MH-S cells (Fig. 5D). Furthermore, flow cytometry experimental result confirmed that compound **6** could suppress IL-6 secretion as well (Fig. 5E). These results illustrated the anti-pneumonia potential of compound **6** *in vitro*.

2.4. Inactivation of NF-κB and MAPK/AP-1 pathways by compound **6** *alleviated pneumonia*

Inflammatory conditions such as pneumonia are critically governed by the activity of the NF-κB and MAPK/AP-1 pathways [48, 49]. To elucidate the underlying molecular mechanism for its efficacy in fighting pneumonia, the regulatory effect of compound **6** toward NF-κB and MAPK/AP-1 pathways were investigated. LPS stimulation significantly activated NF-κB and MAPK pathways (Fig. 6A), as evidenced by increased phosphorylation levels of p65, p38, ERK, and JNK, whereas compound **6** can prevent their phosphorylation for downregulating expressions of downstream protein iNOS and COX-2 (Figs. 6B and 6C). Meanwhile, we performed immunofluorescence experiment for staining p65 (green) and COX-2 (red), and found that green-labeled p65 entered into the nucleus and red-labeled COX-2 were increased after LPS administration, while these results were reversed by compound **6** (Fig. 6A). AP-1, the complex of c-Jun and c-Fos, served as the transcription factor of MAPK pathway to execute a regulatory role. Fig. 6D showed that compound **6** repressed c-Jun and c-Fos expressions in LPS-exposed MH-S cells, which was supported by immunofluorescence staining results (Fig. 6E). Therefore, the anti-pneumonia mechanism of compound **6** involved NF-κB and MAPK/AP-1 pathways.

3. Conclusions

In conclusion, the investigation of chemical constituents of *I. britannica* enabled the successful isolation of seven new compounds (inulabritanoids P–V, **1**–**7**) and thirteen known compounds (**8**–**20**). Compounds **3**, **5**, **6**, **12**, and **18** showed potent anti-pneumonia activities in LPS-exposed MH-S cells. Mechanistically, compound **6** demonstrated significant anti-pneumonia efficacy *in vitro* by blocking NF-κB and MAPK/AP-1 pathways, which illustrated that compound **6** held promise as a prospective lead molecule for the discovery and development of anti-pneumonia medicines, laying a foundation for future studies.

4. Experimental

4.1. General experimental procedures

Bruker AV-600 spectrometer (Bruker, Germany) was used to record NMR data, and signals of CD_3OD, $CDCl_3$, and DMSO-d_6 functioned as references. Botanical samples of *I. britannica* were collected from Shenyang, Liaoning Province, China, with species authentication completed by Prof. Jingming Jia (Shenyang Pharmaceutical University, China).

4.2. Extraction and isolation

Aerial parts of *I. britannica* (8.6 kg) were extracted twice with 95% EtOH followed by 75% EtOH under the same conditions. The combined withdrawals were concentration, subjected to successive extractions with ethyl acetate and *n*-butanol. The fraction (315.8 g) dissolved in ethyl acetate was separated by

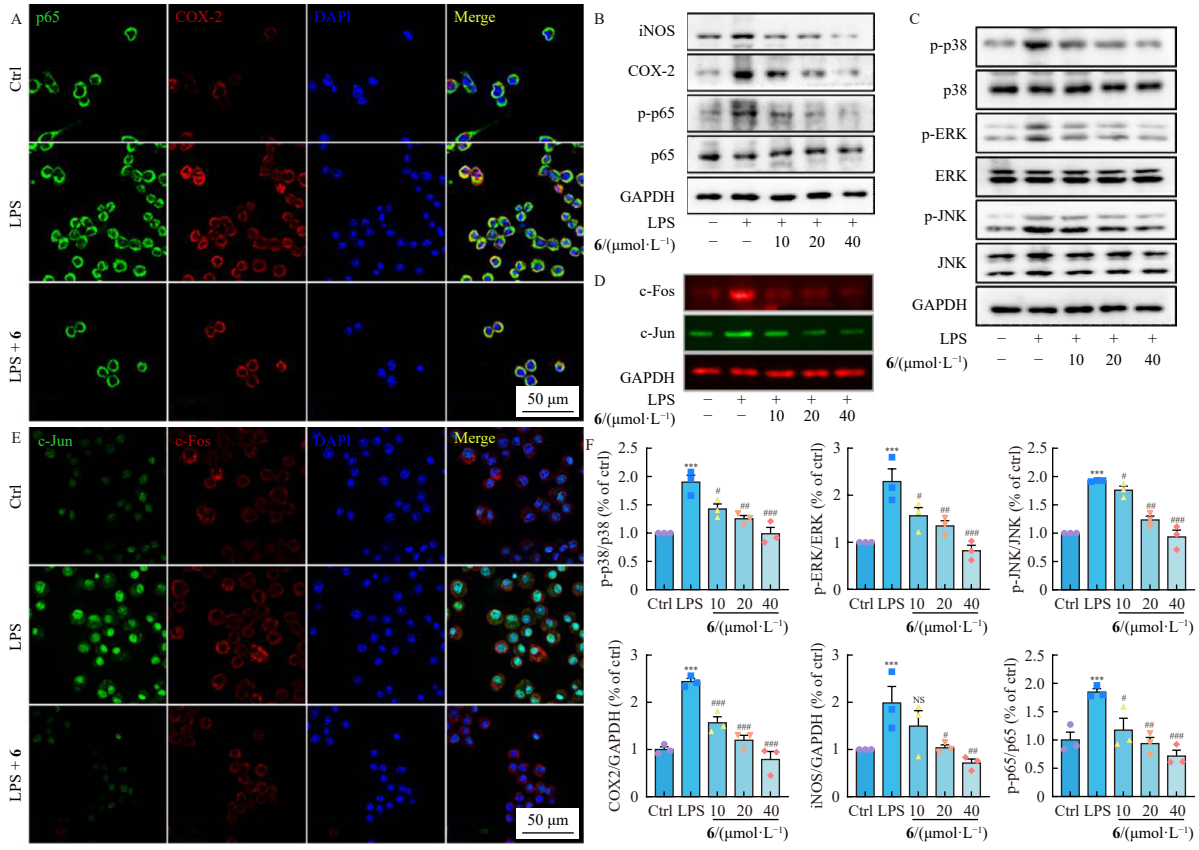


Fig. 6 Compound **6** suppressed the activation of NF-κB and MAPK/AP-1 pathways to exert its anti-pneumonia effect. (A) Immunofluorescence staining of p65 (green) and COX-2 (red); (B–D) Effects of compound **6** toward iNOS, COX-2, p-p65, p65, c-Fos, c-Jun, p-p38, p38, p-ERK, ERK, p-JNK and JNK in LPS-stimulated MH-S cells; (E) Immunofluorescence staining of c-Jun (green) and c-Fos (red); (F) Quantitative data of p-p38/p38, p-JNK/JNK, p-ERK/ERK, COX-2/GAPDH, iNOS/GAPDH, and p-p65/p65. Data were expressed as mean ± SEM (n = 3). $^{***}P < 0.001$ *vs* the control group; $^{\#}P < 0.05$, $^{\#\#}P < 0.01$, $^{\#\#\#}P < 0.001$ *vs* LPS group; NS, no significance, one-way ANOVA.

silica gel column chromatography (CC) and eluted with methylene chloride–methanol (100∶1 to 1∶1), yielding fractions E1–E11. E4 was further purified by a silica gel column and eluted with petroleum ether–acetone (50∶1 to 1∶1) to yield seven sub-components (E41–E47). E43 was refined by polyamide column chromatography and successfully separated three secondary components (E431–E433) using methanol–water gradient elution (50%–90%). Subsequent purification of E432 by ODS CC (10%–90% MeOH) and preparative HPLC (75% CH_3CN) yielded compounds **4** (2.5 mg), **10** (5.8 mg), **11** (10.1 mg), **12** (3.7 mg), and **13** (4.7 mg). Purification of E5 on silica gel (CH_2Cl_2–acetone, 100∶1→1∶1) furnished seven subfractions (E51–E57). Compounds **1** (7.4 mg), **2** (18.5 mg), and **9** (7.2 mg) were obtained from subtraction E53 after ODS CC (MeOH–H_2O, 10%–90%) and preparative HPLC (50% MeOH). E7 was separated by silica gel CC (methylene chloride–methanol, starting ratio of 100∶1 to 4∶1) to yield 15 sub-components (E71–E715). E710 (1.16 g) was processed by silica gel CC using a CH_2Cl_2–MeOH gradient (20∶1→1∶2) and followed by further purification by preparative HPLC with 35% CH_3CN to yield compound **15** (6.9 mg). E712 was separated by silica gel column (CH_2Cl_2–CH_3OH, 18∶1 to 1∶2) and preparative HPLC (26% CH_3CN and 65% CH_3OH) to get compounds **14** (3.0 mg) and **8** (17.8 mg). The *n*-butanol extract (150.0 g) was separated by silica gel CC (CH_2Cl_2–CH_3OH, 50∶1 to 1∶1) to afford 10 fractions (B1–B10). B3 was separated by ODS column (50%–70% CH_3OH) to yield 12 subfractions (B31-B312). B312 was separated by ODS column (10%–100% CH_3OH) and preparative HPLC (40% CH_3CN) to obtain compounds **18** (4.4 mg), **19** (4.2 mg), and **20** (6.1 mg). Purification of B322, B323, B325, and B327 by preparative HPLC (67% CH_3OH for B322; 70% CH_3OH and 50% CH_3CN for B323; 70% CH_3OH for B325; 70% CH_3OH and 50% CH_3CN for B327) to afford compounds **3** (3.6 mg), **5** (3.8 mg), **7** (2.5 mg), **16** (2.7 mg), **17** (3.6 mg), and **6** (3.7 mg).

Inulabritanoid P (**1**): colorless solid; ^1H and ^{13}C data, see Table 1; HR-MS data at *m/z* 335.2211 $[M + H]^+$ (Calcd. for $C_{20}H_{31}O_4^+$, 335.2222).

Inulabritanoid Q (**2**): colorless solid; ^1H and ^{13}C data, see Table 1; HR-MS data at *m/z* 335.2221 $[M - H]^-$ (Calcd. for $C_{20}H_{31}O_4^-$, 335.2222).

Inulabritanoid R (**3**): colorless solid; ^1H and ^{13}C data, see Table 1; HR-MS data at *m/z* 273.1866 $[M + H]^+$ (Calcd. for $C_{18}H_{25}O_2^+$, 273.1855)

Inulabritanoid S (**4**): colorless solid; ^1H and ^{13}C data, see Table 2; HR-MS data at *m/z* 613.3746 $[M - H]^-$ (Calcd. for $C_{36}H_{53}O_8^-$, 613.3740).

Inulabritanoid T (**5**): colorless solid; ^1H and ^{13}C data, see Table 3; HR-MS data at *m/z* 249.1499 $[M + H]^+$ (Calcd. for $C_{15}H_{21}O_3^+$, 249.1491).

Inulabritanoid U (**6**): colorless solid; ^1H and ^{13}C data, see Table 3; HR-MS data at *m/z* 449.1961. $[M - H]^-$ (Calcd. for $C_{27}H_{29}O_6^-$, 449.1964).

Inulabritanoid V (**7**): colorless solid; ^1H and ^{13}C data, see Table 3; HR-MS data at *m/z* 471.2020 $[M + H]^+$ (Calcd. for $C_{26}H_{31}O_8^+$, 471.2019).

4.3. Cell culture

MH-S cells were maintained overnight in RPMI-1640 medium within a humidified incubator set at 37 °C and 5% CO_2. After pre-treatment with compound **6** (10, 20, and 40 μmol·L^{-1}) for 1 h, LPS (1 μg·mL^{-1}) was used for stimulating cells. Subsequently, cell precipitates were collected for further experimental analysis.

4.4. Western blotting

Harvested cell pellets were subjected to lysis in a buffer containing PMSF to obtain total protein extracts. Following electrophoretic separation, proteins were transferred to PVDF membranes which were blocked with skim milk. Primary antibody incubation was performed overnight at 4 °C, subsequently followed by secondary antibody incubation at room temperature. To visually present the experimental results, we treated the protein bands with enhanced chemiluminescent (ECL) reagents and then accurately quantified with the help of ImageJ software (Bethesda, USA).

Table 2 ^1H (600 MHz) and ^{13}C NMR (150 MHz) data of compound **4** in $CDCl_3$.

No.	4				
	δ_C	δ_H (*J* in Hz)		δ_C	δ_H (*J* in Hz)
1	36.4	2.58, m	17	35.0	
		1.02, m	18	47.7	2.04, m
2	25.5	1.80, m	19	46.7	1.86, m
		1.63, m			1.19, m
3	80.0	4.53, dd, (11.9, 4.5)	20	35.5	
4	38.5		21	76.3	4.78, dd, (12.2, 4.8)
5	51.5	1.24, m	22	41.4	1.51, m
6	24.8	2.58, m			1.39, m
		1.79, m	23	27.3	0.95, s
7	75.3	5.17, dd, (11.1, 5.0)	24	17.7	0.83, s
8	44.9		25	179.7	
9	47.0	1.84, m	26	8.9	1.17, s
10	47.8		27	25.8	1.23, s
11	25.5	2.17, dt, (18.2, 4.9)	28	28.3	0.88, s
		1.95, m	29	18.4	0.93, s
12	122.8	5.27, dd, (4.2, 2.5)	30	29.1	0.88, s
13	143.7		OAc-3	171.0	
14	44.0			28.5	2.04, s
15	28.3	1.98, m	OAc-7	170.6	
		1.04, m		22.1	2.02, s
16	21.5	2.04, m	OAc-21	171.1	
				21.4	2.05, s

4.5. Quantitative real-time PCR

After total RNA extraction with Trizol, cDNA was generated *via* reverse transcription. Target genes were analyzed by real-time qPCR using a 2 × SYBR Green system and specific primer sets.

4.6. Immunofluorescence

After supernatant removal, MH-S cells were cleaned with PBS, followed by fixation with pre-chilled methanol and sealing with 5% BSA. Subsequently, cells were separately incorporated with primary antibodies at 4 °C overnight. The following day, samples underwent treatment with fluorescently labeled secondary antibodies, the cell nucleus is colored with DAPI. Finally, imaging and analysis were performed using Leica DM6B thunder system (Leica, Germany).

Table 3 ^{1}H (600 MHz) and ^{13}C NMR (150 MHz) data of compounds **5**–**7** in DMSO-d_6.

No.	5		6		7	
	δ_C	δ_H (J in Hz)	δ_C	δ_H (J in Hz)	δ_C	δ_H (J in Hz)
1	46.9	2.84, q, (8.2)	138.2		122.6	
2	30.0	1.79, m	110.4	6.60, d, (3.7)	129.1	
		1.67, m				
3	34.6	1.92, m	158.4		116.1	6.46, s
		1.21, m				
4	38.8	1.92, m	132.0		147.8	
5	53.9	1.81, m	124.9	6.50, dd, (7.6, 3.7)	144.3	
6	80.4	4.25, q, (9.5)	120.6	6.53, d, (7.6)	116.4	6.87, s
7	50.0	2.97, m	20.9	2.15, s	137.5	7.52, s
8	64.3	4.23, m	58.8		134.1	
9	44.8	2.39, dd, (13.0, 4.4)	103.8	6.20, d, (5.7)	166.2	
		2.29, dd, (13.1, 4.0)				
10	145.1		35.6	2.79, dd, (12.8, 4.1)	63.8	4.06, t, (6.5)
				1.45, m		4.06, t, (6.5)
11	136.8				30.3	1.56, m
						1.56, m
12	169.8				18.6	1.32, m
						1.32, m
13	120.9	6.12, d, (3.4)			13.6	0.88, t, (7.4)
		5.63, d, (2.9)				
14	114.5	4.90, br s				
		4.87, br s				
15	20.2	1.07, d, (5.9)				
1'			68.2		121.1	
2'			83.8	4.43, d, (7.5)	114.6	6.32, d, (2.0)
3'			46.8	2.60, m	144.9	
4'			138.8		143.9	
5'			134.5		115.4	6.57, d, (8.2)
6'			25.1	2.88, dd, (15.4, 2.6)	117.9	6.26, dd, (8.2, 2.0)
				1.92, m		
7'			44.0	0.84, m	44.8	4.24, d, (3.0)
8'			80.7	3.95, td, (12.2, 2.6)	47.8	3.71, d, (3.1)
9'			35.1	1.88, m	172.0	
				1.37, m		
10'			26.0	2.53, m	64.0	3.93, m
						3.93, m
11'			139.9		30.1	1.41, m
						1.40, m
12'			169.4		18.4	1.19, m
						1.19, m
13'			118.0	5.83, d, (3.4)	13.5	0.81, t, (7.3)
				5.56, d, (3.1)		
14'			19.1	0.91, d, (7.0)		
15'			13.2	1.93, s		
OAc-2'			169.8			
			20.8	2.07, s		

4.7. Flow cytometry

Following PBS washing, MH-S cells were collected and fixed with methanol. The fixed samples were then blocked with 5% BSA. Subsequently, incubation was performed with IL-6, followed by FITC-conjugated goat anti-rabbit IgG secondary antibody (SF134, Solarbio). Finally, sample analysis was performed using a CytoFlex flow cytometry (Beckman, USA).

Funding

This work was supported by the National Key R&D Program of China (No. 2025YFC3512700), the National Natural Science Foundation of China (Nos. 82274069, 82504984, and 82505198), the Support Program for Young Faculty's Research and Innovation Capability Development in Tianjin Higher Education Institutions Initiated by the Ministry of Education, the Outstanding Youth Foundation of Tianjin (No. 25JCJQJC00180), the Science Foundation of Tianjin (No. 25JCYBJC00620), the Young Scientific and Technological Talents (Level Two) in Tianjin (No. QN2023-0212), the Tianjin Education Commission Research Program Project (No. 2024KJ004), and the Eaglet Plan Project of Tianjin University of Traditional Chinese Medicine (No. XJS2024101).

Declaration of competing interest

These authors have no conflict of interest to declare.

References

1 Ruuskanen O, Lahti E, Jennings LC. Viral pneumonia. *Lancet*. 2011;377 (9773):1264-1275. https://doi.org/10.1016/S0140-6736(10)61459-6.
2 Mikami K, Suzuki M, Kitagawa H, et al. Efficacy of corticosteroids in the treatment of community-acquired pneumonia requiring hospitalization. *Lung*. 2007;185(5):249-255. https://doi.org/10.1007/s00408-007-9020-3.
3 Tang Y, Shi C, Sun L, et al. Herb pair of Glycyrrhiza Radix–Platycodonis Radix alleviates respiratory syncytial virus pneumonia in mice by modulating lipid metabolism and inhibiting inflammation. *World J Tradit Chin Med*. 2024;10 (3):322-333. https://doi.org/10.4103/wjtcm.wjtcm_79_24.
4 Huang HP, Chen ZP, He XY, et al. Early continuous blood purification affects TNF-α, IL-1β, and IL-6 in patients with severe acute pancreatitis *via* inhibiting TLR4 signaling pathway. *Kaohsiung J Med Sci*. 2022;38(5):479-485. https://doi.org/10.1002/kjm2.12497.
5 Meloche S, Pouysségur J. The ERK1/2 mitogen-activated protein kinase pathway as a master regulator of the G_1- to S-phase transition. *Oncogene*. 2007;26(22):3227-3239. https://doi.org/10.1038/sj.onc.1210414.
6 Zhang J, Zhang M, Zhu QM, et al. Allosteric regulation of Keap1 by 8*β*-hydroxy-*α*-cyclocostunolide for the treatment of acute lung injury. *Acta Pharm Sin B*. 2024;14(9):4174-4178. https://doi.org/10.1016/j.apsb.2024.06.025.
7 Zhu MH, Qi DX, Chen DL, et al. Joint screening and identification of potential targets of nitazoxanide by affinity chromatography and label-free techniques. *Curr Drug Targets*. 2024;25(12):819-845. https://doi.org/10.2174/0113894501297697240805103744.
8 Zhang J, Zhang M, Huo XK, et al. Macrophage inactivation by small molecule wedelolactone *via* targeting sEH for the treatment of LPS-induced acute lung injury. *ACS Cent Sci*. 2023;9(3):440-456. https://doi.org/10.1021/acscentsci.2c01424.
9 Huang HS, Wang M, Guo ZM, et al. Rutaecarpine alleviates acute pancreatitis in mice and AR42J cells by suppressing the MAPK and NF-κB signaling pathways *via* calcitonin gene-related peptide. *Phytother Res*. 2021;35(11): 6472-6485. https://doi.org/10.1002/ptr.7301.
10 Wang K, Zhang P, Sun H, et al. Dual-function natural products: farnesoid X receptor agonist/inflammation inhibitor for metabolic dysfunction-associated steatotic liver disease therapy. *Chin J Nat Med*. 2024;22(11):965-976. https://doi.org/10.1016/S1875-5364(24)60706-5.
11 Chang J, Sun CP, Wang MM, et al. Berberine inhibits phagocytosis through the TLR4-PI3K-CDC42 pathway. *Acta Mater Med*. 2025;4(2):280-292. https://doi.org/10.15212/amm-2024-0074.
12 Zhang J, Zhang WH, Morisseau C, et al. Genetic deletion or pharmacological inhibition of soluble epoxide hydrolase attenuated particulate matter 2.5 exposure mediated lung injury. *J Hazard Mater*. 2023;458:131890. https://doi.org/10.1016/j.jhazmat.2023.131890.
13 Zhang J, Yang XT, Zhang M, et al. Discovery of soluble epoxide hydrolase inhibitors based on the skeleton of piperine: synthesis, properties, molecular dynamics simulation, and their potentials in acute lung injury. *Acupunct Herb Med*. 2025;5(2):193-204. https://doi.org/10.1016/j.ijbiomac.2025.141704.
14 Zhang J, Luan ZL, Huo XK, et al. Direct targeting of sEH with alisol B alleviated the apoptosis, inflammation, and oxidative stress in cisplatin-induced acute kidney injury. *Int J Biol Sci*. 2023;19(1):294-310. https://doi.org/10.7150/ijbs.78097.
15 Zhang J, Zhang HL, Xu XR, et al. Targeting PBK with small-molecule 1-*O*-acetyl-4*R*,6*S*-britannilactone for the treatment of neuroinflammation. *Proc Natl Acad Sci U S A*. 2025;122(29):e2502593122. https://doi.org/10.1073/pnas.2502593122.
16 Cao LJ, Xie HT, Chu ZX, et al. Protective effect of Shenfu Injection against sepsis-induced acute lung injury by suppressing inflammation and apoptosis through the regulation of the janus kinase 2/signal transducer and activator of transcription 3 pathway. *ACS Appl Energy Mater*. 2024;10(4):528-534. https://doi.org/10.4103/wjtcm.wjtcm_76_24.
17 Liao Q, Wu S, Li X, et al. Danggui Niantong Decoction attenuates synovial fibrosis through regulating PI3k/AKT signaling pathway. *J Ethnopharmacol*. 2025;342:119381. https://doi.org/10.1016/j.jep.2025.119381.
18 Yuan JQ, Li XY, Fan YN, et al. Rosmarinic acid suppresses the progression of COPD *via* Syk by modulating airway inflammation and epithelial apoptosis *in vivo* and *in vitro*. *J Asian Nat Prod Res*. 2025;27(5):732-746. https://doi.org/10.1080/10286020.2024.2403617.
19 Chen Y, Zhang XW, Zhao MM, et al. Chlorogenic acid targets SLC37A2 to inhibit macrophage activation *via* ER-dependent NF-κB and NLRP3 signaling pathways against sepsis-induced acute lung injury. *J Asian Nat Prod Res*. 2026;28(3):469-490. https://doi.org/10.1080/10286020.2025.2506181.
20 Sun CP, Jia ZL, Huo XK, et al. Medicinal inula species: phytochemistry, biosynthesis, and bioactivities. *Am J Chin Med*. 2021;49(2):315-358. https://doi.org/10.1142/S0192415X21500166.
21 Yoon HJ, Park JY, Min SJ, et al. *Inula britannica* exerts antioxidant and anti-inflammatory effects in SH-SY5Y cells through the Nrf2-Keap1 signaling pathway. *Arch Biochem Biophys*. 2025;773:110597. https://doi.org/10.1016/j.abb.2025.110597.
22 Meng Z, Li M, Wang X, et al. *Inula britannica* ameliorates alcohol-induced liver injury by modulating SIRT1-AMPK/Nrf2/NF-κB signaling pathway. *Chin Herb Med*. 2024;16(4):667-678. https://doi.org/10.1016/j.chmed.2023.12.006.
23 Zhang HL, Wang N, Shi XL, et al. Sesquiterpenoids from *Inula britannica* and their potential mechanism for immunomodulation. *Phytochemistry*. 2025;231:114343. https://doi.org/10.1016/j.phytochem.2024.114343.
24 Jin HZ, Lee D, Lee JH, et al. New sesquiterpene dimers from *Inula britannica* inhibit NF-κB activation and NO and TNF-α production in LPS-stimulated RAW264.7 cells. *Planta Med*. 2006;72(1):40-45. https://doi.org/10.1055/s-2005-873189.
25 Zhang J, Yan JK, Dong HJ, et al. Dimeric sesquiterpenoids with anti-inflammatory activities from *Inula britannica*. *Chin J Nat Med*. 2025;23(8): 961-971. https://doi.org/10.1016/S1875-5364.
26 Guo C, Qi RY, Ren JY, et al. Inubritantrimers A–D: trimerized sesquiterpenoid [4 + 2] adducts featuring a distinctive Spiro-polycyclic scaffold from *Inula britannica*. *J Org Chem*. 2024;89(7):5029-5037. https://doi.org/10.1021/acs.joc.4c00248.
27 Ibadullayeva AK, Kasela M, Kozhanova KK, et al. Chemical profile and biological properties of methanolic and ethanolic extracts from the aerial parts of *Inula britannica* L. growing in central Asia. *Molecules*. 2024;29(23): 5749. https://doi.org/10.3390/molecules29235749.
28 Gu X, Sun W, Hu Z. Natural products from untapped sources as a potent reserve against antimicrobial resistance crisis. *Chin J Nat Med*. 2024;22(7): 577-579. https://doi.org/10.1016/s1875-5364(24)60610-2.
29 Ma Y, Liu S, Zhou Q, et al. Approved drugs and natural products at clinical stages for treating Alzheimer's disease. *Chin J Nat Med*. 2024;22(8):699-710. https://doi.org/10.1016/s1875-5364(24)60606-0.
30 Chen S, Dai B, Zhang D, et al. Advances in intelligent mass spectrometry data processing technology for *in vivo* analysis of natural medicines. *Chin J Nat Med*. 2024;22(10):900-913. https://doi.org/10.1016/s1875-5364(24)60687-4.
31 Wu ZL, Li JY, Huang PL, et al. New *ent*-kaurane diterpenoid acids from *Nouelia insignis* Franch and their anti-inflammatory activity. *RSC Adv*. 2022; 12(18):11155-11163. https://doi.org/10.1039/d2ra01684b.
32 Cunha WR, Martins C, Ferreira DS, et al. *In vitro* trypanocidal activity of triterpenes from Miconia species. *Planta Med*. 2003;69(5):470-472. https://doi.org/10.1055/s-2003-39719.
33 Zhang L, Shao YL, Hua L, et al. Guaianolides and elemanolides from *Vernonia anthelmintica*. *Phytochem Lett*. 2014;7:14-18. https://doi.org/10.1016/j.phytol.2013.09.009.
34 Zhang XF, Ren J, Cheng XR, et al. One new unusual sesterterpenoid and four new sesquiterpene dimers from *Inula britannica*. *RSC Adv*. 2015;5(3):1979-1982. https://doi.org/10.1002/chin.201522236.
35 Xiao L, Huang YY, Wang YH, et al. Anti-neuroinflammatory benzofurans and lignans from *Praxelis clematidea*. *Fitoterapia*. 2020;140:104440. https://doi.org/10.1016/j.fitote.2019.104440.
36 Wang SJ, Yu M, Li H, et al. Structures and biological activities of polyacylated *ent*-kaurane diterpenoid glycosides from the aerial parts of *Inula hupehensis*. *J Nat Prod*. 2022;85(1):185-195. https://doi.org/10.1021/acs.jnatprod.1c00947.
37 Monsalve LN, Rosselli S, Bruno M, et al. Enzyme-catalysed transformations of *ent*-kaurane diterpenoids. *Eur J Org Chem*. 2005;10:2106-2115. https://doi.org/10.1002/ejoc.200400862.
38 Ying Q, Zhang XX, Xu YK. Chemical constituents of *Alisma orientalis*. *Chem Nat Comp*. 2014;49(6):1143-1145. https://doi.org/10.1007/s10600-014-0844-9.
39 Mahato SB, Kundu AP. ^{13}C NMR spectra of pentacyclic triterpenoids—a compilation and some salient features. *Phytochemistry*. 1994;37(6):1517-1575. https://doi.org/10.1016/S0031-9422(00)89569-2.
40 Dai JQ, Zhao CY, Zhang Q, et al. Taraxastane-type triterpenoids from *Saussurea petrovii*. *Phytochemistry*. 2001;58(7):1107-1111. https://doi.org/10.1016/s0031-9422(01)00397-1.
41 Davidyants ÉS, Putieva ZM, Bandyukova VA, et al. Triterpene glycosides of *Silphium perfoliatum* III. Structure of silphioside E. *Chem Nat Comp*. 1984;

20(6):708-710. https://doi.org/10.1007/BF00580030.
42 Vargas D, Dominguez XA, Acuña-Askar K, et al. Norditerpenes and norditerpene glycosides from *Drymaria arenarioides*. *Phytochemistry*. 1988; 27(5):1532-1534. https://doi.org/10.1016/0031-9422(88)80233-4.
43 Wu YC, Hung YC, Chang FR, et al. Identification of *ent*-16*β*,17-dihydroxykauran-19-oic acid as an anti-HIV principle and isolation of the new diterpenoids annosquamosins A and B from *Annona squamosa*. *J Nat Prod*. 1996;59(6):635-637. https://doi.org/10.1021/np960416j.
44 Wang Y, Hamburger M, Gueho J, et al. Antimicrobial flavonoids from *Psiadia trinervia* and their methylated and acetylated derivatives. *Phytochemistry*. 1989;28(9):2323-2327. https://doi.org/10.1016/S0031-9422(00)97976-7.
45 cIto K, Iita T. Seven sesquiterpene lactones from *Inula britannica* var. chinensis. *Phytochemistry*. 1981;20:271-273. https://doi.org/10.1016/0031-9422(81)85105-9.
46 Doskotch RW, Hufford CD, EI-Feraly FS. Antitumor agents. VI. Sesquiterpene lactones tulipinolide and epitulipinolide from *Liriodendron tulipifera*. *J Org Chem*. 1972;37(17):2740-2744. https://doi.org/10.1021/jo00982a025.
47 Silva J, Alves C, Martins A, et al. Loliolide, a new therapeutic option for neurological diseases? *In vitro* neuroprotective and anti-inflammatory activities of a monoterpenoid lactone isolated from *Codium tomentosum*. *Int J Mol Sci*. 2021;22(4):1888. https://doi.org/10.3390/ijms22041888.
48 Zhao QR, Zhao RH, Geng ZH, et al. Xuanfei Baidu Granule alleviates coronavirus-induced pneumonia in low-temperature and high-humidity environments. *Acupunct Herb Med*. 2023;3(3):200-206. https://doi.org/10.1097/HM9.0000000000000068.
49 Sun CP, Zhou JJ, Yu ZL, et al. Kurarinone alleviated Parkinson's disease *via* stabilization of epoxyeicosatrienoic acids in animal model. *Proc Natl Acad Sci U S A*. 2022;119(9):e2118818119. https://doi.org/10.1073/pnas.2118818119.



The cover design illustrates the discovery of anti-pneumonia compounds from *Inula britannica*. The red-colored lung on the left represents the inflamed state induced by lipopolysaccharide (LPS) challenge, whereas the blue-colored lung on the right symbolizes the protective outcome following treatment with inulabritanoid U. A row of *I. britannica* at the bottom releases glowing particles, indicating the bioactive extracts from this natural source, which exert a protective effect on the lung, with inulabritanoid U being the most potent among them. Within the left lung, an alveolar macrophage is depicted, and a ball-and-stick model of inulabritanoid U directly targets this cell, highlighting that this agent exerts its therapeutic effect against pneumonia by suppressing LPS-mediated inflammation in non-epithelial MH-S cells. This narrative reflects the focus on bioactive natural products from TCM, their mechanisms, and lead compound development. By integrating natural product chemistry with pharmacology, this study advances TCM-derived therapeutics against acute respiratory inflammation.